

1 **Cohesive and mixed sediment in the Regional Ocean**
2 **Modeling System (ROMS v3.6) implemented in the**
3 **Coupled Ocean Atmosphere Wave Sediment-Transport**
4 **Modeling System (COAWST r1179): Supplement**

5
6 Christopher R. Sherwood¹, Alfredo Aretxabaleta¹, Courtney K. Harris², J. Paul
7 Rinehimer^{2, 3}, Bénédicte Ferré^{1, 4}, Romaric Verney⁵

8 ¹U. S. Geological Survey, 384 Woods Hole Road, Woods Hole, MA 02543-1598 USA

9 ²Virginia Institute of Marine Sciences, Gloucester Point, Virginia, USA

10 ³Currently at WEST Consultants, Bellevue, WA, USA

11 ⁴IFREMER, Plouzane, France

12 ⁵Currently at CAGE-Centre for Arctic Gas Hydrate, Environment, and Climate;
13 Department of Geosciences, UiT The Arctic University of Norway, N-9037 Tromsø,
14 Norway

15
16 *Correspondence to:* Christopher R. Sherwood (csherwood@usgs.gov)

17 **1 Introduction**

18 This Supplement provides additional details and formulae describing the cohesive- and
19 mixed-sediment algorithms, and a guide to variables and keywords used to control model
20 options. Some of the material from the main paper is repeated here to aid readability.

21
22 This supplement describes parts of the COAWST implementation of ROMS version 3.6
23 (COAWST Subversion revision 1179, distributed by the U.S. Geological Survey. Contact
24 jcwarner@usg.gov). The source code for ROMS is distributed among several directories.

25 Most of the code dealing with sediment is in the directory

26 COAWST\ROMS\Nonlinear\Sediment. This includes the non-cohesive routines developed
27 as part of the Community Sediment-Transport Modeling System (CSTMS) and described
28 by Warner et al., 2010, and the new cohesive and mixed-bed routines described in the
29 main paper. Two example applications are provided in the

30 COAWST\Projects\Sed_floc_toy and COAWST\Projects\Sedbed_toy folders.

32 Many ROMS options are specified using keywords parsed by the C Pre-processor (CPP)
 33 routine prior to model program compilation. These keywords are selected by users in
 34 application-dependent include (or header; .h) files. In this supplement, keywords are
 35 denoted in UPPER_CASE, and file names are denoted with `monospace` font. Table S1
 36 provides a list of the notation used in the equations and Table S2 lists the associated
 37 ROMS variable names as they appear in input or output files. Table S3 lists ROMS
 38 variables required in the input files, and Table S4 lists ROMS variables used to track
 39 seabed properties.

40 **2 Model Algorithms**

41 The sediment algorithms implemented as part of ROMS follow the schematic presented
 42 in Figure S1. The water-column dynamics are coupled with the sediment dynamics at
 43 each model time step. Inside the sediment module, the main routine (`sediment.F`)
 44 controls the execution of the user-selected sediment behavior options. Separate routines
 45 calculate bottom-boundary layer hydrodynamics (wave-current interaction,
 46 hydrodynamic roughness, and bed shear stresses), bedload transport, suspended-sediment
 47 settling, flocculation and disaggregation, erosion and deposition, and changes in bed
 48 sediment properties.

49 The new contributions that simulate cohesive and mixed sediment include a floc model
 50 for particle flocculation and disaggregation in the water column, and several procedures
 51 for cohesive and mixed behavior in the seabed.

52 *2.1 Floc Model*

53 The floc model FLOCMOD of Verney et al. (2011) is implemented in the ROMS routine
 54 `sed_flocs.F`. FLOCMOD treats a finite number (NCS, Number of Cohesive Sediment
 55 classes) of size classes with representative floc diameters D_f (m). The model assumes
 56 that floc densities ρ_f (kg/m^3) decrease with size, and are related to the primary
 57 disaggregated particle diameter D_p (m) and density ρ_s (kg/m^3) through a fractal
 58 dimension n_f (dimensionless; Kranenburg, 1994) according to

$$59 \quad \rho_f = \rho_w + (\rho_s - \rho_w) \left(\frac{D_f}{D_p} \right)^{n_f - 3} \quad (\text{S } 1)$$

60 where ρ_w (kg/m^3) is the density of the interstitial water in the flocs (Table 1). The mass
 61 m (kg) of an individual floc is therefore

62
$$m = \rho_s \frac{\pi}{6} D_p^3 \left(\frac{D_f}{D_p} \right)^{n_f} \quad (\text{S } 2)$$

63 The fractal dimension for natural flocs is typically close to 2.1 (Tambo and Watanabe,
 64 1979; Kranenburg, 1994). Floc densities increase as n_f increases, and at $n_f = 3$, the flocs
 65 are solid particles with $\rho_f = \rho_s$. When the floc model is used in ROMS (CPP keyword
 66 SED_FLOCS is defined), all cohesive sediment classes are treated as flocs and the
 67 processes of aggregation and disaggregation can act to shift mass of suspended sediment
 68 from one class to another.

69 Users are responsible for providing cohesive sediment parameters in the input file
 70 `sediment.in` that are consistent with Equation (S 1). An example is provided in
 71 `COAWST\Projects\Sed_floc_toy\sediment_sed_floc_toy.in`. Verney et al. (2011)
 72 report that at least eight floc classes were required to reproduce the results of their lab
 73 experiment.

74 FLOCMOD simulates two-particle interactions that result in aggregation after collisions
 75 caused by either shear or differential settling, and disaggregation caused by turbulence
 76 shear and/or collisions. The rate of change in the number concentration $N(k)$ (m^{-3}) of
 77 particles in the k^{th} floc class is controlled by a coupled set of linear equations

78
$$\frac{dN(k)}{dt} = G_a(k) + G_{bs}(k) + G_{bc}(k) - L_a(k) - L_{bs}(k) - L_{bc}(k) \quad (\text{S } 3)$$

79 where k is the particle class, and G ($\text{m}^{-3} \text{s}^{-1}$) and L ($\text{m}^{-3} \text{s}^{-1}$) terms represent gain and loss
 80 of mass by the three processes denoted by subscripts: a (aggregation), bs (breakup caused
 81 by shear), and bc (breakup caused by collisions). Equations (S 3) are integrated explicitly
 82 using adjustable time steps that may be as long as the baroclinic model time step, but are
 83 decreased automatically when necessary to ensure that particle number concentrations
 84 remain positive. Particle number concentrations $N(k)$ are related to suspended mass
 85 concentrations $C_m(k)$ (kg/m^3) via the mass of the individual flocs m as

86
$$N(k) = C_m(k) / m(k) \quad (\text{S } 4)$$

87 The aggregation terms in Equations (S 3) include gain in class k caused by collisions
 88 between classes i and j

89
$$G_a(k) = \frac{1}{2} \sum_{i+j=k} \alpha_{ij} A(i, j) N_i N_j \quad (\text{S } 5)$$

90 and loss from class k by accretion into class i

91
$$L_a(k) = \sum_1^N \alpha_{ij} A(i, k) N_i N_k \quad (\text{S } 6)$$

92 where α is the collision efficiency and $A(i, j)$ is the probability function for two-particle
 93 shear-induced collisions between classes i and j . In general, the collision efficiency
 94 depends on environmental factors (temperature, salinity) and the nature (shape, mineral
 95 composition, organic-matter content, etc.) of the two particle classes, but in our
 96 implementation, a universal collision efficiency is used. The probability of shear-induced
 97 collision depends on the particle diameters D_f (m) and the shear rate $G = \sqrt{\varepsilon / \nu}$ (s^{-1}),
 98 where ε (m^2/s^3) is the turbulence dissipation rate and ν (m^2/s) is the kinematic viscosity
 99 of the fluid:

100
$$A(i, j) = \frac{1}{6} G (D_i + D_j)^3 \quad (\text{S } 7)$$

101 FLOCMOD includes terms for collisions caused by differential settling but, because shear-
 102 induced collisions are much more effective in turbulent environments, we have not
 103 exercised that part of the code.

104 The turbulence dissipation rate ε is computed from the turbulence submodel in ROMS.
 105 For example, when the generic length scale equation (Umlauf and Burchard, 2002;
 106 Warner et al., 2005) is used

107
$$\varepsilon = \left(c_\mu^0 \right)^{3+gls_p/gls_n} tke^{3/2+gls_m/gls_n} gls^{-1/gls_n} \quad (\text{S } 8)$$

108 where c_μ^0 is the stability coefficient, tke is turbulent kinetic energy, gls is the second,
 109 generic parameter in the turbulence submodel, and gls_p , gls_n , and gls_m are
 110 coefficients that define the submodel. These coefficients are provided as user input,
 111 usually as one of four specific combinations that define one of three classic turbulence
 112 closures or a fourth generic closure of Umlauf and Burchard (2002; see Table 1 in
 113 Warner et al., 2005).

114 The shear-breakup terms in Equations (S 3) for gain or loss in class k due to
 115 fragmentation in larger classes i are

116
$$G_{bs}(k) = \sum_{i=k+1}^n \text{FDBS}_{ki} B_i N_i \quad (\text{S } 9)$$

117 and

118
$$L_{bs}(k) = B_k N_k \quad (\text{S } 10)$$

119 where the fragmentation rate B_i for class i is

120
$$B_i = \beta_i G^{3/2} D_{f,i} \left(\frac{D_{f,i} - D_p}{D_p} \right)^{3-n_f} \quad (\text{S } 11)$$

121 where β_i is a fragmentation rate that depends on the yield strength of the flocs. FDBS is
 122 a function that determines how much of the mass appears in class k when a particle in
 123 class i breaks up due to shear. The exponents in Equation (S 11) follow from
 124 Winterwerp's (2002) assumption that equilibrium floc size is related to the Komogorov
 125 microscale. Three distribution functions are implemented to characterize floc breakup in
 126 FLOCMOD (Verney et al., 2011): binary distribution (flocs break into two equal sizes, each
 127 with half of the mass); ternary distribution (flocs break into three parts, one with half of
 128 the mass, and two with a quarter of the mass); and erosion (flocs break into one large
 129 fragment and n smaller fragments, where the mass of the large fragment is reduced by n
 130 times the mass of the smaller fragments; Hill, 1996). The relative contribution of each of
 131 these breakup distribution functions is controlled by model parameters discussed below.

132 Collision-induced breakup terms in Equations (S 3) are defined as proposed by
 133 McAnally and Mehta (2001) as

134
$$G_{bc}(k) = \sum_{ij} \text{FDBC}_{ij} A(i, j) N_i N_j \quad (\text{S } 12)$$

135
$$L_{bc}(k) = \sum_{i=1}^n \text{FDBC}_{ik} A(i, k) N_i N_k \quad (\text{S } 13)$$

136 where FDBC is the function that determines the distribution of fragments after a
 137 collision. It depends on the collision-induced shear stress τ^{coll} (Pa) and the strength τ^y
 138 (Pa) of the particles. The collision-induced shear stress experienced by particle in class i
 139 during a collision with a particle in class j is

140
$$\tau_{ij,i}^{coll} = \frac{8(G(D_{f,i} + D_{f,j})/2)^2 m_i m_j}{\pi F_p D_i^2 (D_{f,i} + D_{f,j})(m_i + m_j)} \quad (\text{S } 14)$$

141 where F_p is a relative depth of interparticle penetration estimated as $F_p = 0.1$ (Krone,
 142 1963; McAnally, 1999; McAnally and Mehta, 2001). Particle strength depends on floc
 143 density ρ_i :

144
$$\tau_i^y = F_y \left(\frac{\rho_w - \rho_{f,i}}{\rho_w} \right)^{2/(3-n_f)} \quad (\text{S } 15)$$

145 where F_y (Pa) is the floc yield strength, taken as $10^{-10} N$ (Winterwerp and van Kesteren,
 146 2004). If the collision-induced shear stress exceeds the particle strength of only one of the

147 two colliding particles, the weaker particle (class j) breaks into two fragments: a larger
 148 one with mass $13/16m_j$, and a smaller one with mass $3/16m_j$ that binds with the stronger
 149 particle. If the collision-induced stress is greater than the particle strength of both classes,
 150 then each particle breaks into two parts, producing particles with masses $13/16m_i$, $3/16m_i$,
 151 $13/16m_j$, and $3/16m_j$. The smaller fragments bind to form a particle with mass
 152 $3/16m_i+3/16m_j$ (McAnally, 1999; McAnally and Mehta, 2001).

153 *Floc model parameters*

154 The floc model introduces several parameters (Table 2), some of which have been
 155 evaluated by Verney et al. (2011). These parameters are specified by the user as input to
 156 the model in the `sediment.in` file. We have not performed an extensive sensitivity
 157 analysis for these parameters, but others indicate that the equilibrium floc size depends on
 158 the ratio of aggregation to breakup parameters, and the rate of floc formation and
 159 destruction depends on their magnitudes (Winterwerp, 1999; 2002).

160 The diameter, settling velocity, density, critical stress for erosion, and critical stress
 161 for deposition are also specified as inputs for each sediment class (Table 3). We have
 162 assumed, for the cases presented here, a fractal relationship between floc diameter and
 163 floc density (Equation (S 1); Kranenburg, 1994) and a Stokes settling velocity w (m/s):

$$164 \quad w_i = \frac{(\rho_i - \rho_w)gD_{f,i}^2}{18\mu} \quad (\text{S } 16)$$

165 where $\mu \approx 0.001 \text{ Pa} \cdot \text{s}$ is the dynamic viscosity of the fluid. Alternative relationships
 166 between diameter and settling velocity exist, such as modified Stokes formula (e.g.,
 167 Winterwerp, 2002; Winterwerp et al., 2007; Droppo et al., 2005; Khelifa and Hill, 2006).
 168 The relationship between diameter and floc density described in Equation (S 1) cannot be
 169 changed, however, without significant modifications to portions of the model code that
 170 ensure mass conservation as sediment changes classes during aggregation and
 171 disaggregation.

172 *Fluxes into the bed – Critical shear stress for deposition*

173 The settling flux of flocs (and all other size classes) into the bed (deposition) over a time
 174 step is calculated as $w_i \rho_i C_{v,i} \Delta t$, where w_i , ρ_i , and $C_{v,i}$ are the settling velocity, floc (or
 175 particle) density, and volume concentration for the i^{th} size class in the bottom-most water-
 176 column layer, respectively, and Δt is the model time step. ROMS calculates the settling
 177 flux in `sed_settling.F`. The concept of a critical stress for deposition τ_d (Pa) (Krone,

178 1962; Whitehouse et al., 2000; Mehta, 2014) has been implemented as an option; if
 179 selected, deposition is zero when the bottom stress τ_b exceeds τ_d , and increases linearly
 180 as τ_b decreases below τ_d (Whitehouse et al., 2000), as follows.

$$181 \quad \begin{aligned} & (1 - \tau_b / \tau_{d,i}) w_i \rho_i C_{v,i} \Delta t \quad \text{for } \tau_b < \tau_{d,i} \\ & 0 \quad \text{for } \tau_b \geq \tau_{d,i} \end{aligned} \quad (\text{S } 17)$$

182 We call this linear depositional flux, and it is invoked with CPP option
 183 SED_TAU_CD_LIN.

184 A simpler alternative is to assume a full settling flux when $\tau_b < \tau_d$, which we call
 185 constant depositional flux:

$$186 \quad \begin{aligned} & w_i \rho_i C_{v,i} \Delta t \quad \text{for } \tau_b < \tau_{d,i} \\ & 0 \quad \text{for } \tau_b \geq \tau_{d,i} \end{aligned} \quad (\text{S } 18)$$

187 which is invoked with SED_TAU_CD_CONST. The calculations are performed in
 188 `sed_fluxes.F`. The critical stress for deposition for each size class $\tau_{d,i}$ for both cohesive
 189 and non-cohesive classes must be specified as input; large values effectively nullify the
 190 calculation, particularly when using the constant depositional flux (Equation (S 18)).

191 Earlier versions of the CSTMS included these input variables as placeholders but did not
 192 use them. There is not a consensus on specifying τ_d . According to Whitehouse et al.
 193 (2000), τ_d is typically about one-half the magnitude of the critical shear stress for erosion
 194 τ_c , but is unrelated to that value. Mehta (2014, Equation 9.83) suggests

$$195 \quad \tau_d = \tau_{dp} \left(D_{f,i} / D_p \right)^\xi \quad (\text{S } 19)$$

196 where τ_{dp} is τ_d for the smallest particle diameter D_p and ξ is an exponent that depends
 197 on sediment properties. Mehta (2014) lists values of $\tau_{dp} = 0.03$ Pa and $\xi = 0.5$ for
 198 kaolinite with $D_p = 1 \mu\text{m}$, citing Letter (2009) and Letter and Mehta (2011). The effect
 199 of either Equation (S 17) or Equation (S 18) when $\tau_b \geq \tau_d$ is to prevent deposition and
 200 keep sediment in suspension in the bottom layer. This allows the material to be
 201 transported as suspended sediment and, for flocs, allows aggregation and disaggregation
 202 processes to continue.

203 *Changes in floc size distribution within the bed*

204 It seems reasonable to expect changes in the size-class distribution of flocs once they
 205 have been incorporated into the seabed, in contrast to non-cohesive particles that retain
 206 their properties during cycles of erosion and deposition. For example, it seems unlikely
 207 that large, low-density flocs can be buried and later resuspended intact, and limited

208 published observations suggest that material deposited as flocs can be eroded as denser,
 209 more angular aggregates (Stone et al., 2008). However, we find little guidance for
 210 constraining this process. We therefore have implemented a simple formulation that
 211 allows the user to stipulate an equilibrium cohesive size-class distribution and an
 212 associated relaxation time scale, as described below. The user-specified equilibrium
 213 distribution controls the size classes in the bed that are resuspended when cohesive bed
 214 material is eroded.

215 The calculations to specify changes to floc distribution in the bed are made in
 216 `sed_bed_cohesive.F` when the CPP option `SED_DEFLOC` is invoked. The equilibrium
 217 fractional distribution f_{ceq} of the cohesive size classes in the bed is specified as input. In
 218 bed layers (except the top, active layer), the equilibrium mass distribution is calculated as

$$219 \quad m_{eq,i} = f_{ceq,i} m_{tot} \quad (\text{S } 20)$$

220 where m_{tot} is the sum of the mass in all of the cohesive classes in that bed layer:

$$221 \quad m_{tot} = \sum_{i=1}^{\text{NCS}} m_i \quad (\text{S } 21)$$

222 where NCS is the number of cohesive classes. The floc distribution in a layer is nudged
 223 toward the equilibrium distribution according to

$$224 \quad m_i^{new} = m_i^{old} + c(m_{eq,i} - m_i^{old}) \quad (\text{S } 22)$$

225 where the nudging coefficient c is determined by the model time step Δt and the user-
 226 specified time scale t_{eq} as

$$227 \quad c = \min(1, \Delta t / t_{eq}) \quad (\text{S } 23)$$

228 This formulation conserves mass, but does not achieve full equilibrium unless $t_{eq} \leq \Delta t$.
 229 Test cases presented in Section 3 of the main paper demonstrate the effect of this process
 230 and the associated time scale on floc distributions both in the bed and in the water
 231 column.

232 *2.2 Properties of sediment, seafloor, and seabed.*

233 The model accounts for two distinct types of sediment: non-cohesive sediment (e.g.,
 234 sand) and cohesive sediment (e.g., mud). The general framework is unchanged from
 235 Warner et al. (2008), except that the expanded model requires additional variables to
 236 allow for both cohesive and non-cohesive types. The number of sediment classes of each
 237 type is, at present, limited to twenty-two by input/output formatting protocols. The total

238 number of sediment classes, NSED, equals the sum of the number of non-cohesive
239 (NNS) and cohesive (NCS) classes. At least one class of one type is required for
240 sediment-transport modeling. Classes may be used to represent sediment with a range of
241 properties that are specified by the user, and remain constant throughout the model
242 calculations. Sediment properties are stored in two one-dimensional arrays (one for non-
243 cohesive sediment and one for cohesive sediment) and include particle diameter,
244 sediment density, settling velocity, critical shear stress for erosion, critical shear stress for
245 deposition (this value is presently ignored for non-cohesive sediment), erosion-rate
246 coefficient, and porosity (Table 3).

247 Seafloor properties describe the condition of the sediment surface and are stored in
248 arrays with two spatial dimensions that correspond to the horizontal model domain
249 (Warner et al., 2008). Seafloor properties (Table S4) include representative values
250 (geometric means) of sediment in the top layer, including grain size, critical shear stress
251 for erosion, settling velocity, and density; and properties of the sediment surface, such as
252 ripple height, ripple wavelength, and bottom roughness. These properties may be
253 specified as input, or calculated in the model. The arrays are also used to store additional
254 parameters if cohesive or mixed sediment calculations are being performed, as discussed
255 below.

256 Seabed properties (i.e. stratigraphy) are stored with three spatial dimensions
257 representing horizontal location and layer in the bed. As with other model dimensions,
258 the number of layers used to represent seabed properties (NBED) is specified in user
259 input files and remains constant throughout the model run. Each sediment bed layer
260 stores information, including the mass of each sediment class, porosity, and age. The
261 layer thickness, which is derived from mass and sediment density for each class and
262 porosity, is stored for convenience, as is the depth to the bottom of each layer. To account
263 for consolidation and swelling, the framework used in Warner et al. (2008) with
264 modifications discussed in the next section, has been augmented to store additional
265 information for bulk critical shear stress τ_{cb} in each bed layer if cohesive sediment
266 formulations are enabled with CPP keywords COHESIVE_BED or MIXED_BED.

267 *2.3 Stratigraphy*

268 Representation of seabed properties, i.e. the stratigraphy, has been modified slightly from
269 the framework presented in Warner et al. (2008). Here we summarize the overall scheme
270 for the sediment bed layers, emphasizing the modifications to the model beyond the
271 Warner et al. (2008) framework.

272 Stratigraphy serves two functions in the model as conditions change and sediment is
273 added or removed from the bed: (1) to represent the mixture of sediment available at the
274 sediment-water interface for use in bedload transport, sediment resuspension, and
275 roughness calculations; and (2) to record the depositional history of sediment. Algorithms
276 for tracking and recording stratigraphy must conserve sediment mass and must accurately
277 record and preserve age, porosity, and other bulk properties that apply to each layer.
278 Ideally, a layer could be produced for each time step in which deposition occurs, and a
279 layer could be removed when cumulative erosion exceeds layer thickness. In practice, the
280 design of many models (including ROMS) adds an additional constraint: the number of
281 layers (NBED) used to record stratigraphy is declared at the beginning of the model run
282 and cannot change. Thus, when deposition creates a new layer, or when erosion removes
283 a layer, layers must be merged and split so that the total number of layers remains equal
284 to NBED. Where and when this is done determines the fidelity and utility of the modeled
285 stratigraphic record. Some models have used a constant layer thickness (Harris and
286 Wiberg, 2001); others (for example, ECOMSED) define layers as isochrons deposited
287 within a fixed time interval (HydroQual, Inc., 2004). Our approach is most similar to that
288 described by Le Hir et al. (2011) in that we allow mixing of deposited material into the
289 top layer, and require a minimum thickness of newly formed layers, merging the bottom
290 layers when a new layer is formed.

291 A key component of the bed model is the active layer (Hirano, 1971), which is the
292 thin (usually mm-scale), top-most layer of the seabed that participates in exchanges of
293 sediment with the overlying water. During each model time step, deposition and erosion
294 may contribute or remove mass from the active layer. One disadvantage of this approach
295 is that any stratigraphy in the active layer is lost by instantaneous mixing (Merkel and
296 Klopman, 2012), but this is consistent with the original concept of Hirano (1971) and
297 the need to represent the spatially averaged surface sediment properties in a grid cell that
298 represents a heterogeneous seabed. For non-cohesive sediment, Warner et al. (2008) set
299 the active-layer thickness $\Delta z_a = \max[k_1(\tau_{sf} - \langle \tau_c \rangle), 0] + k_2 \langle D \rangle$, where τ_{sf} (Pa) is the skin
300 friction component of the wave-current combined bottom shear stress, and $\langle \tau_c \rangle$ (Pa) is
301 the critical shear stress for erosion of the particles in the active layer, $\langle D \rangle$ (m) is the
302 representative diameter of particles in the active layer, and k_1 and k_2 are dimensional
303 empirical coefficients with values of 0.007 and 6, respectively (Harris and Wiberg, 1997).
304 The brackets indicate that $\langle \tau_c \rangle$ and $\langle D \rangle$ are determined as the fraction-weighted
305 geometric mean from contents of the active layer at the end of the previous time step.
306 When COHESIVE_BED is enabled, the active layer thickness is defined as the depth

307 where the bulk critical shear stress of the sediment bed exceeds the bottom shear stress,
308 so sediment is available for resuspension in the layer $z < z_p$ where $\tau_b > \tau_{cb}(z_p)$. When
309 MIXED_BED is enabled, the active layer thickness is calculated using both methods, and
310 the greater of the two values is used.

311 The bed model conserves mass and maintains a constant number of layers (NBED),
312 even during erosional or depositional cycles. The thickness of the top layer at the start of
313 each time step is equal to the active-layer thickness Δz_a determined during the previous
314 step. These are unchanged from Warner et al., 2008. However, improved fidelity of the
315 stratigraphic record is obtained with a revised sequence of layer calculations that occur
316 when COHESIVE_BED, MIXED_BED, or (for non-cohesive simulations) SED_BED2
317 is enabled, as follows. (1) Mass associated with deposition or erosion of each class is
318 added or subtracted to the top layer. Erosion in each class is limited to the mass of that
319 class available in the active layer. (2) The new Δz_a is calculated, based on stresses from
320 the current time step and sediment properties from the previous time step. (3) If the top
321 layer is thinner than Δz_a , material from sequentially deeper layers is merged to form a
322 top layer with thickness Δz_a . If, instead, the top layer is thicker than Δz_a , excess
323 sediment is placed in the second layer. The user-specified value $\Delta z_{nl\ max}$ is used to
324 constrain the thickness of the second layer during deposition, so that continued deposition
325 produces multiple layers, none of which are thicker than $\Delta z_{nl\ max}$. (4) If deposition requires
326 formation of one or more layers (beneath the top layer), the bottom-most layers are
327 merged to maintain NBED layers. If, on the other hand, layers have been merged, one or
328 more thin layers (with thickness $\Delta z_{nl\ max}$; see below) are split from the bottom layer to
329 maintain NBED layers. The new layers are assigned properties (grain size, porosity, etc.)
330 identical to those of the original bottom layer. Note that the original formulation in
331 Warner et al. (2008) split the bottom layer into equal halves to form an additional layer.
332 (5) The final step in the bed model calculates age and porosity of each layer as mass-
333 weighted arithmetic means. Representative seafloor properties associated with the
334 sediment in the top layer, including $\langle D \rangle$, $\langle \tau_c \rangle$, $\langle w_s \rangle$, and $\langle \rho_s \rangle$ are calculated as
335 geometrical means, weighted by the fractional amount of each sediment class in the layer.

336 The revised bed model gives the user latitude to control the resolution of the bed
337 model through the choice of values for $\Delta z_{nl\ max}$ and NBED, and avoids the mixing
338 described by Merkel and Klopmann (2012). The main differences from previous versions
339 of the model (Warner et al., 2008) are the treatments of the second layer (immediately
340 below the active layer) and the bottom layer. During deposition, the new algorithm
341 prevents the second layer from becoming thicker than $\Delta z_{nl\ max}$, which results in thinner

342 layers that can record changes in sediment composition inherited from the active layer as
 343 materials settle. During erosion, the new algorithm splits off only a small portion of the
 344 bottom layer to create a new layer with thickness $\Delta z_{nl\ max}$ unless the bottom layer is
 345 thinner than $\Delta z_{nl\ max}$, in which case the bottom layer is split. This limits the influence of
 346 the initial stratigraphy specified for the bottom layer and confines blurring of the
 347 stratigraphic record the bottommost layers. Our tests indicate the new approach provides
 348 a more informative record of stratigraphic changes, and Moriarty et al. (2017) used a
 349 similar approach to bed stratigraphy to preserve spatial gradients in sediment
 350 biogeochemistry.

351 2.4 Bulk Critical Shear Stress for Cohesive Sediment

352 When the cohesive bed model is invoked (CPP keyword COHESIVE_BED), the
 353 erodibility depends on the bulk critical shear stress τ_{cb} (Pa), which is a property of the bed
 354 layer, not individual sediment classes. The bulk critical shear stress generally increases
 355 with depth in the bed, and changes with erosion, deposition, swelling, and consolidation.
 356 The cohesive bed model tracks these changes by updating profiles of τ_{cb} at each grid
 357 point and time step.

358 There is no generally accepted physically based model for determining τ_{cb} from bed
 359 properties such as particle size, mineralogy, and porosity. We adopted Sanford's (2008)
 360 heuristic approach based on the concept that the bulk critical shear stress profile tends
 361 toward an equilibrium profile $\tau_{cb\ eq}(z)$ (Figure 1 in main paper). This method tracks only
 362 τ_{cb} instead of directly modeling consolidation, swelling, and other physical process
 363 responsible for altering bed critical stresses. The $\tau_{cb\ eq}$ profile depends on depth in the
 364 seabed and must be determined a priori. Erosion-chamber measurements have been used
 365 to define this equilibrium bulk shear stress profile $\tau_{cb\ eq}$ (Sanford, 2008; Rinehimer et al.,
 366 2008; Dickhudt et al., 2009; Dickhudt et al., 2011; Butman et al., 2014). The equilibrium
 367 bulk shear stress profile is defined using two parameters, *offset* and *slope*:

$$368 \quad \tau_{cb\ eq} = a \exp\left[\left(\ln(z_\rho) - offset\right) / slope\right] \quad (S\ 24)$$

369 where *offset* and *slope* have units of $\ln(\text{kg}/\text{m}^2)$, and $a = 1\ \text{Pa}\ \text{kg}^{-1}\ \text{m}^2$ is a dummy
 370 coefficient that produces the correct units of critical shear stress. The mass depth, z_ρ
 371 (kg/m^2) is the cumulative dry mass of sediment overlying a given depth in the bed, so the
 372 mass depth at the bottom of each model layer k is calculated as

$$373 \quad z_\rho(k) = \sum_{k=1, NBED} \sum_{i=1, NSED} f_{i,k} \rho_i \Delta z_k \quad (S\ 25)$$

374 Equation (S 24) can be related to the power-law fits to erosion-chamber measurements
 375 presented by Dickhudt (2008) and Rinehimer et al. (2008), which take the form

$$376 \quad \tau_{ec} = a' m_{ec}^b \quad (\text{S } 26)$$

377 where m_{ec} is the cumulative mass eroded at an applied erosion-chamber shear stress τ_{ec}
 378 and a' and b are dimensional coefficients, with $slope = 1/b$ and $offset = -slope \ln(a')$. In
 379 the model, the equilibrium stress profile is further bounded with

$$380 \quad \tau_{cbmin} \leq \tau_{cb eq} \leq \tau_{cbmax} \quad (\text{S } 27)$$

381 where the user-provided minimum and maximum values τ_{cbmin} and τ_{cbmax} apply at the
 382 sediment water interface and deep in the sediment, respectively. The instantaneous
 383 profile is nudged toward the equilibrium profile to represent the effects of consolidation
 384 or swelling following perturbations caused by erosion or deposition:

$$385 \quad \frac{\Delta \tau_{cb}}{\Delta t} = \begin{cases} \frac{1}{T_c} (\tau_{cb eq} - \tau_{cb}), & \tau_{cb} < \tau_{cb eq} \\ 0, & \tau_{cb} = \tau_{cb eq} \\ -\frac{1}{T_s} (\tau_{cb eq} - \tau_{cb}), & \tau_{cb} > \tau_{cb eq} \end{cases} \quad (\text{S } 28)$$

386 where T_c (s) is the time scale for consolidation and T_s (s) is the time scale for swelling.
 387 The consolidation time scale is usually chosen to be much shorter ($T_s \sim 10^{-2} T_c$) than the
 388 one associated with swelling (Sanford, 2008). New sediment deposited to the surface
 389 layer is assigned a bulk critical shear stress that may either be (1) held constant at a low
 390 value (Rinehimer et al. 2008), or (2) set at the instantaneous bed shear stress of the flow.

391 *2.5 Mixed Sediment*

392 The mixed-sediment algorithm is intended to ensure reasonable behavior when both
 393 cohesive and non-cohesive sediment are present in a model domain. The algorithm
 394 depends on the mud fraction in the bed. Beds with low mud content behave according to
 395 rules for non-cohesive sediment and erodibility is determined by critical shear stress of
 396 the particles present in the active layer. Non-cohesive beds may be winnowed and
 397 armored by selective erosion of the finer fraction. In contrast, beds with high mud content
 398 behave according to bulk properties that, in the model, are characterized by the bulk
 399 critical shear stress for erosion. Mixed beds have intermediate mud content and their
 400 critical shear stress in the model is a weighted combination of cohesive and non-cohesive
 401 values.

402 We define a cohesive-behavior parameter P_c (dimensionless) that characterizes the
 403 extent to which the bed sediment behaves cohesively. Where $P_c = 0$, there is no cohesive
 404 behavior, and the effective critical shear stress τ_{ce} for each sediment class is used as the
 405 particle shear stress τ_c for that class. Where $P_c = 1$, the cohesive sediment algorithm is
 406 used, and the effective critical shear stress for each class is the greater of τ_{ce} and the bulk
 407 critical shear stress τ_{cb} . Between those limits, the effective critical shear stress for each
 408 sediment class is

$$409 \quad \tau_{ce} = \max \left[P_c \tau_{cb} + (1 - P_c) \tau_c, \tau_c \right] \quad (\text{S } 29)$$

410 The overall proportion of sediment in cohesive classes f_c in the active mixed layer
 411 determines the cohesive behavior parameter P_c :

$$412 \quad f_c = \frac{\sum_{i=1, NCS} f_i \rho_i}{\sum_{i=1, NCS} f_i \rho_i + \sum_{i=1, NNS} f_i \rho_i} \quad (\text{S } 30)$$

413 where f_c quantifies the overall mud content in the bed, f_i is the volume fraction, and ρ_i is
 414 the sediment grain density of sediment class i . Material behaves non-cohesively ($P_c = 0$).
 415 where $f_c \leq f_{nc \text{ thresh}}$. Typical values of $f_{nc \text{ thresh}}$ are $\sim 0.03 - 0.10$, indicating that a cohesive
 416 sediment content of more than a few percent changes the behavior of the bed (Mitchener
 417 and Torfs, 1996; Panagiotopoulos et al., 1997; van Ledden et al., 2004; Jacobs et al.,
 418 2011). Completely cohesive behavior occurs when f_c exceeds $f_{c \text{ thresh}}$ which typically has
 419 values of $\sim 0.20 - 0.30$. Between those limits, P_c changes linearly:

$$420 \quad P_c = \begin{cases} 0, & f_c \leq f_{nc \text{ thresh}} \\ \min \left[\max \left(\frac{f_c - f_{nc \text{ thresh}}}{f_{c \text{ thresh}} - f_{nc \text{ thresh}}}, 0 \right), 1 \right], & f_{nc \text{ thresh}} < f_c < f_{c \text{ thresh}} \\ 1, & f_c \geq f_{c \text{ thresh}} \end{cases} \quad (\text{S } 31)$$

421 This approach allows fine material (e.g., clay) to be easily resuspended when only a small
 422 fraction of mud is present in an otherwise sandy bed, and it limits the flux to the amount
 423 available in the active mixed layer. It also allows non-cohesive silt or fine sand embedded
 424 in an otherwise muddy bed to be resuspended during bulk erosion events, and it provides
 425 a simple and smooth transition between these behaviors. The thickness of the active
 426 mixed layer is calculated as the thicker of the cohesive and non-cohesive estimates. The
 427 behavior is discussed in Section 3 of the main paper and illustrated in Figure 3.

428 2.6 Bed Mixing

429 Mixing of bed properties in sediment can be caused by infauna (ingestion, defecation, or
 430 motion such as burrowing) or circulation of porewater, and tends to smooth gradients in
 431 stratigraphy and move material vertically in sediment. The model assumes that mixing is
 432 a vertical diffusive process and neglects non-local mixing processes; see Boudreau
 433 (1997) for a more complete discussion of mixing models for sediment. Mixing is
 434 described by the diffusion equation

$$435 \quad \frac{\partial C_v}{\partial t} = \frac{\partial}{\partial z} \left(D_b \frac{\partial C_v}{\partial z} \right) \quad (\text{S } 32)$$

436 where C_v (m^3/m^3) is the volume concentration of a conservative property (e.g., fractional
 437 concentration of sediment classes or porosity), D_b is a (bed-depth-dependent)
 438 (bio)diffusion coefficient (m^2/s), and z (m) is depth in the bed (zero at the sediment-water
 439 interface, positive downward). Zero-flux boundary conditions are imposed at the top and
 440 bottom of the sediment bed, and a fully implicit numerical solution is used that is
 441 unconditionally stable and conserves bed properties.

442 The depth-dependent biodiffusion coefficient profile in the model can be specified for
 443 each horizontal grid cell. The shape of the profile $D_b(z)$ is specified using five parameters,
 444 as follows (Figure S2).

$$445 \quad D_b = \begin{cases} D_{bs}, & z \leq z_s \\ D_{bs} \exp\left(\frac{-z - z_s}{r}\right), & z_s < z \leq z_m \\ D_{bm} - \frac{D_{bm}}{z_{zero} - z_m} (z - z_m), & z_m < z \leq z_{zero} \\ \sim 0, & z > z_{zero} \end{cases} \quad (\text{S } 33)$$

446 where

$$447 \quad r = \frac{-z_m - z_s}{\log(D_{bm} / D_{bs})} \quad (\text{S } 34)$$

448 where z_s , z_m , and z_{zero} are depths in the bed (m). D_{bs} represents the biodiffusivity from the
 449 surface to depth z_s , and is the value used for the biodiffusion coefficient to depth z_s .

450 Between depths z_s and z_m , the biodiffusion coefficient decreases exponentially from D_{bs}
 451 to D_{bm} . Between depths z_m and z_{zero} , biodiffusivity decreases linearly from D_{bm} to a small
 452 background value, where it remains below z_{zero} . Uniform, exponential, and linear portions
 453 of the profile can be expanded, contracted, or eliminated by manipulating z_s , z_m , and z_{zero} .

454 This method of defining the biodiffusivity profile was chosen for flexibility and has been
 455 used to represent sediment mixing on the Palos Verdes shelf, CA (Sherwood et al., 2002),
 456 and the Rhone subaqueous delta (Moriarty et al. 2017).

457 We evaluated the numerical characteristics of the implemented biodiffusion
 458 algorithm. The convergence and sensitivity was tested by comparing numerical solutions
 459 with known analytical solutions (Fisher et al., 1979) for two cases (not shown): point-
 460 source diffusion (Dirac case) and diffusion across a step in concentration (Heaviside
 461 case). The solution was accurate to first order with truncation error governed by the time
 462 step and square of the layer thickness. For typical time steps used in regional-scale ocean
 463 models (~seconds to minutes) and ~mm- to cm-scale bed layer thickness, the numerical
 464 solution behaved well. The algorithm conserved mass and also behaved appropriately for
 465 non-uniform bed thicknesses and for spatially variable diffusivities.

466 **Tables**

467 Table S1. List of symbols

<i>Symbol</i>	<i>Description</i>	<i>Typical or Default Value Used Here</i>	<i>Units</i>
<i>A</i>	Probability function for two-particle collision among floc classes <i>i</i> and <i>j</i>		–
<i>B</i>	Fragmentation rate		1/s
<i>C_v</i>	Volume concentration		m ³ / m ³
<i>C</i>	Mass concentration		kg / m ³
<i>D</i>	Sediment (non-cohesive or cohesive) diameter	4e-6 – 2e-3	m
<i>D_b</i>	Sediment (bio)diffusivity		m ² / s
<i>D_{bs}</i>	Sediment (bio)diffusivity at sediment-water interface		m ² / s
<i>D_{bm}</i>	Sediment (bio)diffusivity at bottom of exponential profile		m ² / s
<i>D_f</i>	Floc diameter	4e-6 – 2e-3	m
<i>D_p</i>	Primary particle diameter	4e-6 – 20e-6	m
<i>E</i>	Erosion rate		kg m ⁻² s ⁻¹

E_0	Erosion rate parameter	$\sim 0.005 - 0.05$	$\text{kg m}^{-2} \text{s}^{-1}$
$FDBC$	Floc distribution function due to collision breakup		–
$FDBS$	Floc distribution function due to shear breakup		–
F_p	Relative depth of interparticle (floc) penetration	0.1	–
F_y	Floc yield strength	10^{-10}	N
G	Turbulence shear rate	$\sim 0 - 20$	1/s
G_a	Gain rate in floc class by aggregation		$\text{m}^{-3}\text{s}^{-1}$
G_{bc}	Gain rate in floc class by collision breakup		$\text{m}^{-3}\text{s}^{-1}$
G_{bs}	Gain rate in floc class by shear breakup		$\text{m}^{-3}\text{s}^{-1}$
L_a	Loss rate from floc class by aggregation		$\text{m}^{-3}\text{s}^{-1}$
L_{bc}	Loss rate from floc class by collision breakup		$\text{m}^{-3}\text{s}^{-1}$
L_{bs}	Loss rate from floc class by shear breakup		$\text{m}^{-3}\text{s}^{-1}$
M	Erosion rate parameter	$\sim 0.005 - 0.05$	$\text{kg m}^{-2} \text{s}^{-1}$ $\text{Pa}^{-1} \text{m}^{-2}$
N	Number concentration of floc particles		m^{-3}
NBED	Number of bed layers	1 to unlimited	–
NCS	Number of cohesive sediment classes	0 to unlimited	–
NNS	Number of non-cohesive sediment classes	0 to unlimited	–
NSED	Total number of sediment classes (NCS+NNS)	at least 1	–
P_c	Cohesive behavior parameter	0 to 1	–
T_c	Time scale for consolidation	$\sim 0 - 360,000$	s

T_s	Time scale for swelling	$100 \times T_c$	s
a	dummy coefficient in (3 and S 24)	1	$\text{Pa kg}^{-1} \text{m}^{-2}$
a'	dimensional coefficient in (S 26)	$\sim 1 - 5$	m s^2
b	non-dimensional coefficient	$\sim 0.3 - 0.6$	–
c	Nudging coefficient	0 – 1	–
c_μ^0	Stability coefficient in turbulence model	varies depending on turbulence model	Table 2. in Warner et al. (2005)
f	Volume fraction of sediment class	0 – 1	–
f_c	Mass fraction of cohesive material in bed	0 – 1	–
f_{ceq}	Equilibrium fractional distribution of cohesive sediment	0 – 1	–
$f_c \text{ thresh}$	Mass fraction threshold for fully cohesive behavior	0.2	–
$f_{nc \text{ thresh}}$	Mass fraction threshold for fully non-cohesive behavior	0.03 – 0.1	–
g	Gravitational acceleration	9.81	m/s^2
gls	Second (length-scale) parameter in GLS turbulence model	varies depending on turbulence model	Table 1. in Warner et al. (2005)
gls_m	Coefficient in GLS turbulence model	"	"
gls_n	Coefficient in GLS turbulence model	"	"
gls_p	Coefficient in GLS turbulence model	"	"
h	Water depth	5 - 20	m
i	Index	1 to NBED, 1 to NCS	–
j	Index	1 to NBED, 1 to NCS	–
k	Index	1 to NBED, 1 to NCS	–
k_1	Coefficient in active-layer formula	0.007	m / Pa
k_2	Coefficient in active-layer formula	6	–
m	Floc mass		kg

m_{ec}	Cumulative mass eroded in erosion chamber		kg
m_{eq}	Equilibrium sediment mass		kg
m_{tot}	Total mass of sediment		kg
n_f	Fractal dimension	1.9 – 2.2	–
$offset$	Coefficient in equilibrium critical shear stress for erosion profile		$\ln(\text{kg}/\text{m}^2)$
r	Denominator in biodiffusivity profile equation		m
s	Sea-surface elevation		m
$slope$	Coefficient in equilibrium critical shear stress for erosion profile		$\ln(\text{kg}/\text{m}^2)$
t	Time		s
t_{eq}	Equilibrium time scale		s
Δt	Model time step	1 – 100	s
tke	Turbulence kinetic energy		m^2/s^2
u	Water velocity	0 – 2	m/s
u^*	Shear velocity	0 – 0.05	m/s
w_s	Settling velocity	$10^{-5} - 10^{-3}$	m/s
x	Distance		m
z	Depth in sediment bed; Elevation above seafloor	0 – 2; 0 - 20	m
z_m	Depth in sediment to bottom of exponential biodiffusive mixing	0.005 – 0.10	m
z_s	Depth in sediment to bottom of exponential biodiffusive mixing	0.01 – 0.5	m
z_{zero}	Depth in sediment to bottom of biodiffusive mixing	0.02 - 2	m
z_0	Bottom roughness length	$10^{-5} - 10^{-2}$	m
z_ρ	Mass depth in sediment bed		kg/m^2

Δz	Bed-layer thickness	10^{-3} to 10^0	m
Δz_a	Active-layer thickness	10^{-4} to 10^{-2}	m
$\Delta z_{nl\ max}$	Maximum layer thickness	10^{-4} to 10^{-2}	m
α	Collision efficiency	0.35	–
β	Fragmentation rate coefficient	0.15	–
ε	Turbulence dissipation rate		m^2/s^3
κ	von Kármán's constant	0.41	–
μ	Dynamic viscosity	0.001	Pa s
ξ	Exponent coefficient	0.5	–
ρ_s	Particle density of sediment	2650	kg / m^3
ρ_f	Floc density	1200 - 2650	kg / m^3
ρ_w	Water density	1030	kg / m^3
τ_b	Bottom shear stress		Pa
τ_c	Critical shear stress for erosion		Pa
τ_{cb}	Bulk critical shear stress for erosion of cohesive bed		Pa
$\tau_{cb\ eq}$	Equilibrium bulk critical shear stress for erosion		Pa
$\tau_{cb\ min}$	Equilibrium bulk critical shear stress for erosion		Pa
$\tau_{cb\ max}$	Equilibrium bulk critical shear stress for erosion		Pa
τ_{ce}	Effective critical shear stress for erosion of mixed sediment		Pa
τ^{coll}	Floc collision induced shear stress		Pa
τ_d	Critical shear stress for deposition		Pa
τ_{dp}	Critical shear stress for deposition of the primary particles	0.03	Pa

τ_{ec}	Erosion chamber shear stress		Pa
τ_{sf}	Skin-friction component of bottom shear stress		Pa
τ^y	Floc strength		Pa
ν	Kinematic viscosity	10^{-6}	m^2/s

468

469

470 Table S2. Variables associated with the floc model FLOCMOD as implemented in
 471 ROMS/CSTMS, listed in order of appearance in the sediment.in input file.

<i>Symbol in Text</i>	<i>Model Variable Name in FLOCMOD</i>	<i>Description</i>	<i>Typical or Default Value</i>	<i>Units</i>
	l_ADS	Enable differential settling	F	True/False
	l_ASH	Enable shear aggregation	T	True/False
D_p	f_dp0	Primary particle size	4e-6	m
	f_dmax	Maximum particle size	Not used	m
	f_nb_frag	Number of fragments by shear erosion	2	-
α	f_alpha	Flocculation efficiency (range: 0 – 1)	0.35	-
β	f_beta	Shear fragmentation rate (0 – 1)	0.15	-
	f_ater	Ternary breakup: 0.5; Binary: 0.0	0.0	-
	f_ero_frac	Fraction of shear fragmentation term transferred to shear erosion (0 – 1)	0.0	-
	f_ero_nbfrag	Number of fragments induced by shear erosion	2.0	-
	f_ero_iv	Fragment size class	1	-
	f_collfragparam	Fragmentation rate for collision- induced breakup	0.01	-
	f_clim	Min. concentration below which floc processes are not calculated	0.001	kg / m ³
	l_testcase	Set G values to Verney et al. (2011) values	F	True/False
	MUD_FRAC_EQ	Fractional size class distribution for cohesive sediment in bed		NNS values; sum must be unity.
	t_dfloc	Time scale for deflocculation in bed	200.0	s

472

473

474 Table S3. Sediment property parameters stored for each sediment class in ROMS. These
 475 are defined by the user in an input file with the generic name `sediment.in`.

<i>Symbol</i>	<i>Array Name^a</i>	<i>Description</i>	<i>Typical Range of Values</i>	<i>Units</i>
D	SD50	Median sediment grain diameter	10^{-4} - 10	mm
m	CSED	Sediment concentration	0 - 20	kg / m ³
ρ	SRHO	Sediment grain density	2650	kg / m ³
w	WSED	Particle settling velocity	10^{-2} - 100	mm / s
E_0	ERATE	Erosion rate coefficient	10^{-3} - 10^{-2}	kg m ⁻² s ⁻¹
τ_{ce}	TAU_CE	Critical shear stress for erosion	0.02 - 5	Pa = N / m ²
τ_d	TAU_CD	Critical shear stress for erosion	Not well constrained	Pa = N / m ²
ϕ	POROS	Porosity	0.1 - 0.9	m ³ / m ³

476 ^aArray names are preceded by either SAND_ or MUD_ for non-cohesive and cohesive
 477 sediment, respectively.

478

479 Table S4. Seabed properties stored at each horizontal grid cell in the BOTTOM array in
 480 ROMS/COAWST.

<i>Symbol</i> (<i>this paper</i>)	<i>Array Index</i> (<i>Name (in model)</i>)	<i>Description</i>	<i>Typical or Default Value</i> <i>for parameters introduced in this paper</i>	<i>Units</i>
D_r	isd50	Representative grain diameter ^a		m
$\langle \rho_s \rangle$	idens	Representative sediment density ^a		kg / m ³
$\langle w_s \rangle$	iwsed	Representative particle settling velocity ^a		kg / m ³
$\langle \tau_{ce} \rangle$	itauc	Representative critical shear stress for erosion (kinematic units)		m ² / s ²
	irlen	Ripple wavelength		m
	irhgt	Ripple height		m
	ibwave	Near-bottom wave-orbital excursion amplitude		m
	izdef	Default bottom roughness		m
	izapp	Apparent bottom roughness		m
	izNik	Nikuradse bottom roughness		m
	izbio	Biological bottom roughness		m
	izbfm	Bedform bottom roughness		m
	izbld	Saltation bottom roughness		m
	izwbl	Bottom roughness used in wave model		m
z_a	iactv	Active-layer thickness		m
	ishgt	Saltation height		m
	idefx	Erosion flux		kg m ⁻² s ⁻¹

idnet	Net erosion or deposition		kg m ⁻²
idoff	Offset for erodibility profile ^b	[-0.469, 0.3]	
idslp	Slope of erodibility profile ^b	[1.7, 2]	
idtim	Equilibrium time scale for erodibility profile ^b	[2, 8, 24] hours	s
idbmx	Bed biodiffusivity maximum ^c	[10 ⁻¹⁰ , 10 ⁻⁵]	m ² / s
idbmm	Bed biodiffusivity minimum ^c	[10 ⁻¹² , 10 ⁻⁸]	m ² / s
idbzs	Depth to bottom of uniform biodiffusivity profile ^c	0.002	m
idbzm	Depth to bottom of linear biodiffusivity profile ^c	0.08	m
idbzp	Depth to bottom of non-zero biodiffusivity profile ^c	0.01	m
idprp	Cohesive behavior ^d	0-1	-

481 ^aCalculated as a fraction-weighted geometric mean.

482 ^bOnly required for cohesive or mixed sediment calculations.

483 ^cOnly required for bed mixing.

484 ^dOnly required for mixed sediment calculations.

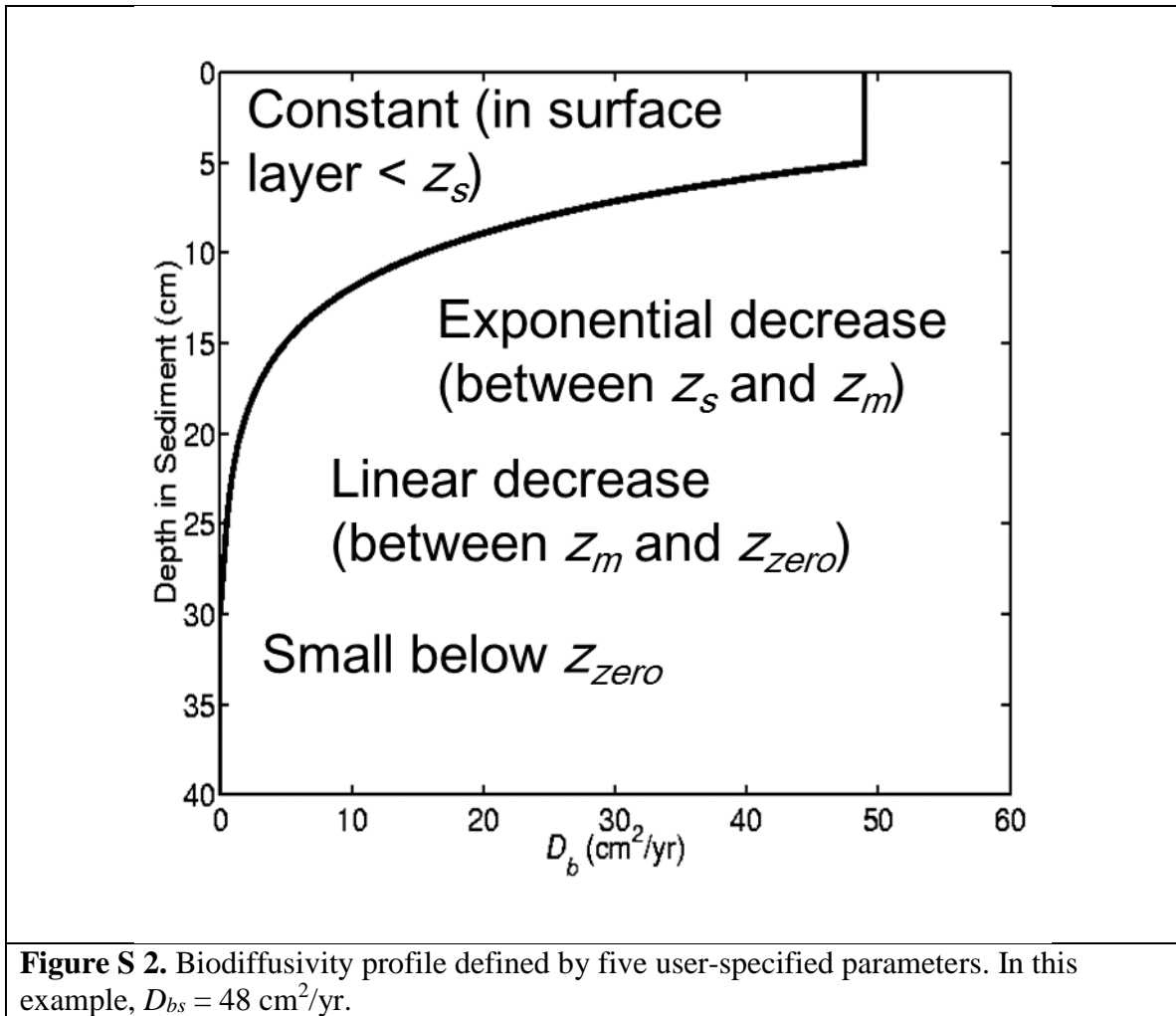
485

```

if SEDIMENT
  sediment.F - Initiate sediment routines
  if BEDLOAD
    sed_bedload.F - Bedload transport
  endif
  if SUSPLOAD
    if SED_FLOCS
      sed_flocs.F - Floc dynamics
    endif
    sed_settling.F - Suspended sediment settling
    sed_fluxes.F - Erosion / Deposition
  endif
  if COHESIVE_BED or MIXED_BED
    sed_bed_cohesive.F *- Cohesive / mixed stratigraphy
    if SED_FLOCS and SED_DEFLOC
      sed_bed_cohesive.F *- Adjust floc distribution in bed
    endif
  elseif NONCOHESIVE_BED2
    sed_bed2.F *- Non-cohesive stratigraphy (revised)
  else
    sed_bed.F - Non-cohesive stratigraphy (original)
  endif
  if SED_BIODIFF
    sed_biodiff.F* - Biodiffusive mixing of bed
  endif
  sed_surface.F - Update surface properties

```

Figure S 1. Pseudocode describing components of the CSTMS sediment module activated by C preprocessor keywords (**BOLD**) during compilation. Filenames in the source code are indicated with courier font. Components with asterisks (*) are new.



489